I&EC research
Industrial & Engineering Chemistry Research

Article

Cite This: Ind. Eng. Chem. Res. 2019, 58, 22924−22933

pubs.acs.org/IECR

Nitric and Sulfuric Acid Solubility in Dense Phase CO_2

Bjørn H. Morland,*[,†,‡] Adriana Tadesse,[†] Gaute Svenningsen,[†] Ronald D. Springer,[§] and Andre Anderko[§]

[†]Institute for Energy Technology, P.O. Box 40, NO-2027 Kjeller, Norway

[‡]Department of Chemistry, University of Oslo, Gaustadalléen 21, NO-0349 Oslo, Norway

[§]OLI Systems, Inc., 240 Cedar Knolls Rd., Suite 301, Cedar Knolls, New Jersey 07927, United States

ABSTRACT: Research has shown that strong acids (i.e., sulfuric and nitric acids) may be produced as a result of reactions between impurities during CO_2 transport within carbon capture, utilization, and storage (CCUS) systems even when today's impurity specifications and recommendations are followed. Strong acids are corrosive to carbon steel, which is a very common construction material for CO_2 transport pipelines. To establish acceptable impurity limits and to ensure the integrity of pipelines, experimental data are needed as input for modeling possible scenarios and as a foundation for constructing modeling tools. To assess the possibility of formation of concentrated acid-bearing phases in CO_2 environments, acid solubility in dense phase CO_2 needs to be determined. The nitric and sulfuric acid solubilities in dense phase CO_2 were determined by first saturating the CO_2 phase with the acids and by subsequently scrubbing the acids using water-filled autoclaves. The water was then analyzed using ion chromatography. The experiments were conducted at two temperatures (25 and 48 °C) with four different pressures (80, 100, 120, and 170 bar). The new solubility measurements have been used in conjunction with available literature data to construct a thermodynamic model for predicting the thermodynamic behavior of acid−CO_2 mixtures over wide ranges of temperatures, pressures, and compositions. The model is based on the previously developed Mixed-Solvent Electrolyte (MSE) framework and incorporates speciation and phase equilibria in CO_2-rich as well as water-rich environments.

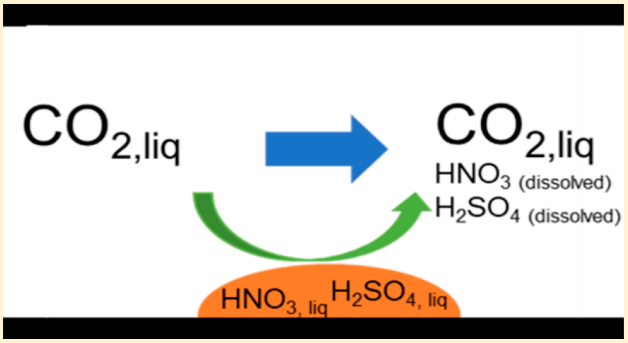

1. INTRODUCTION

The International Energy Agency (IEA)[1] and the Intergovernmental Panel on Climate Change (IPCC)[2] have set a goal to reduce CO_2 emissions to limit the global temperature rise. It is foreseen that carbon capture, utilization, and storage (CCUS) are needed to reach this goal. A key element in the implementation of CCUS is to keep the cost as low as practically possible. For this reason, the captured and compressed CO_2 should not be encumbered with unnecessary and costly cleaning procedures to remove accompanying species, which are called impurities in this paper. Some of these impurities may react and produce strong acids,[3−6] which could cause severe problems in the transportation and storage systems. It is expected that the captured CO_2 will be transported from the capture site to the storage location as bulk cargo (on ships or trains) or in pipelines. For pipeline transport, the material choice has a huge impact on the cost. Corrosion-resistant alloys are expensive and can probably be used only for short pipelines, while carbon steel is the only economically realistic alternative for long pipelines. Corrosion-resistant materials (which are considerably more expensive) can probably be used at the capture site where aggressive species are expected.

To keep the operating costs low, monitoring tools are necessary to predict when or if the integrity of the transportation chain could be threatened. A lot of work has been done to determine safe limits for specific impurities in CO_2 for transport in carbon steel pipelines, but little has been done to implement these results into a tool that can be used to predict when chemical reactions, corrosion, and solid formation could be expected. Crucial in such a tool is the knowledge about reactions, interactions, and solubility of the involved species. Previous work by our research group[4−7] has identified some of the reactions and interactions that could occur at different concentrations of the expected impurities, and it was shown that sulfuric and nitric acids could form under certain conditions. Hoa et al.[8] showed that, at low pressure, the condensation of SO_2 and NO_2 with water resulted in the formation of H_2SO_4 and HNO_3, which led to strong pitting and localized corrosion in the presence of H_2SO_4, while HNO_3 induced only high general corrosion. This might be related to different corrosion mechanisms as both Hoa et al.[8] and Morland et al.[9] suggested, but it could also be an indication of a difference in solubility.

Received: September 5, 2019
Revised: November 7, 2019
Accepted: November 19, 2019
Published: November 19, 2019

DOI: 10.1021/acs.iecr.9b04957
Ind. Eng. Chem. Res. 2019, 58, 22924−22933

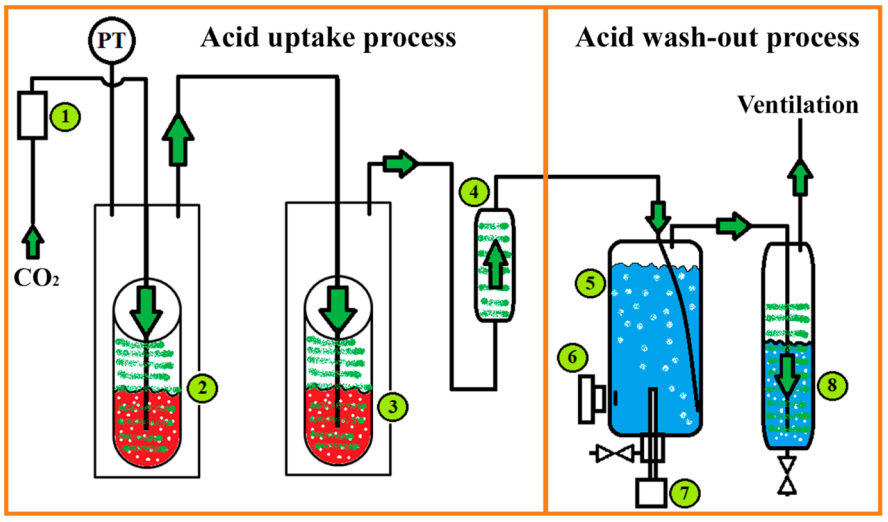

Figure 1. Sketch of the experimental setup: (1) CO_2 expansion/buffer tank, (2 and 3) acid saturation autoclaves, (4) acid droplet fall-out tank, (5) main acid scrubber, (6) magnetic stirrer, (7) conductivity probe, and (8) secondary acid scrubber.

However, no data exist on the solubility of these acids in dense phase CO_2. Such information is important because formation of these acids will create a highly corrosive environment, entailing the risk of rapid corrosion and formation of corrosion products. On the other hand, if the acids remain dissolved in the bulk CO_2 phase, they can probably follow the stream without affecting the transportation pipeline. Therefore, the threshold when the formation of a separate, acid-rich phase occurs (i.e., when the solubility limit is exceeded) needs to be known for a wide range of pressures and temperatures that are relevant to CO_2 transport systems. The existing models available today are not capable of predicting the solubility of these acids due to the lack of experimental data. With accurate solubility data, new specifications and recommendations could be determined if the amount of impurities and the physical properties of the system are known.

In addition to the fundamental measurements in CO_2-rich phases, it is necessary to establish a thermodynamic model for interpolating and extrapolating the measurements over the whole range of conditions that are of practical interest. Most importantly, the model needs to be inherently applicable to multicomponent mixtures and include the behavior of other impurities (such as NO_x, SO_x, H_2O, H_2S, and O_2). Furthermore, it needs to be capable of simulating reactions between the impurity species within both the H_2O-rich and CO_2-rich phases. Such requirements for thermodynamic modeling are unique to CO_2 transportation systems and have not been previously considered in chemical process industries.

Over the past two decades, a tremendous amount of work has been devoted to the development of thermodynamic models for CO_2 systems. These models have been recently reviewed by Span et al.,[10] Munkejord et al.,[11] Trusler,[12] and Bui et al.[13] For the prediction of phase equilibria and other thermodynamic properties of CO_2 and its mixtures with impurities such as N_2, O_2, H_2, or CO, extremely accurate multiparameter equations of state are available. Notably, the well-known GERG model[14] is accurate for CO_2 and various components other than water. A more recent multiparameter equation of state, EOS-CG,[15] was designed specifically for carbon capture and storage and can be used for systems that include water.

Although these models offer the highest accuracy of calculation of volumetric properties and other derived properties, they are inherently not designed for systems involving electrolytes and, therefore, are not suitable for corrosion-related studies. For treating electrolyte systems, various other models have been developed. In general, these models fall into two categories: (1) $\gamma-\varphi$ models, in which activity coefficients (γ) are used to reproduce the properties of aqueous solutions, whereas an equation of state provides fugacity coefficients (φ) to represent the properties of the gas phase and (2) $\varphi-\varphi$ models, in which a homogeneous equation of state reproduces the properties of both the liquid and gas phases. While most of the existing $\gamma-\varphi$ models for CO_2 systems have been developed primarily for calculating the solubility of CO_2 in water and various electrolyte solutions,[16−22] some models have been applied to predict the mutual solubilities of aqueous and CO_2-rich phases.[23] The fundamentals of $\gamma-\varphi$ models for carbon capture and storage have been recently reviewed by Trusler.[12] Also, Li et al.[24,25] compared the performance of $\gamma-\varphi$ and $\varphi-\varphi$ models for CCUS applications. The $\varphi-\varphi$ models either incorporate electrolyte-specific terms in an equation of state that was otherwise developed for nonelectrolytes[26−28] or combine a classical equation of state with an excess Gibbs energy model for electrolytes.[29,30] A particularly notable family of models of this kind is based on the Statistical Associating Fluid Theory (SAFT). Applications of SAFT to CO_2 systems have been reviewed by Bui et al.[13]

For modeling complex electrolyte mixtures in CO_2 environments, the $\gamma-\varphi$ and $\varphi-\varphi$ approaches have their advantages and disadvantages. From a fundamental point of view, the $\varphi-\varphi$ models are more appropriate for systems that can exist in both subcritical and supercritical states because they can reproduce the vapor−liquid critical behavior (at least within the limitations of classical theories). On the other hand, the $\gamma-\varphi$ methods impose a division of the phase space into gas-like and liquid-like regions, which is necessary even for supercritical systems for which there is no inherent boundary between the gas and liquid states. However, the $\gamma-\varphi$ methods are much more suitable when electrolyte speciation and, more generally, chemical equilibria need to be studied in addition to phase equilibria. This is practically necessary whenever chemically reactive species are dissolved in CO_2 phases. For chemically reacting systems, the $\varphi-\varphi$ approach would be computationally impractical due to the need to solve the equation of state in each phase while solving

DOI: 10.1021/acs.iecr.9b04957
Ind. Eng. Chem. Res. 2019, 58, 22924−22933

phase equilibrium conditions and ensuring the chemical equilibrium constraints in both the water-rich and CO_2-rich phases.

To study the formation of corrosive species in CO_2 transportation, it is essential to have a thermodynamic model that predicts both phase and chemical equilibria not only in the water-rich phase but also in the CO_2-rich phase. This requirement is satisfied by the previously developed Mixed-Solvent Electrolyte (MSE) model,[31,32] which has been designed in the $\gamma-\varphi$ framework for the simultaneous calculation of phase and chemical equilibria in systems containing strong and weak electrolytes in aqueous, nonaqueous, and mixed solvents. This model has been found to be accurate for CO_2-H_2O-salt systems, for which it predicts pH as a manifestation of acid−base equilibria[33] as well as the compositions of both the aqueous and CO_2-rich phases.[32] Also, the model reproduces both the speciation and vapor−liquid equilibria of strong acids at concentrations ranging from infinite dilution in water to pure acids and even to pure acid anhydrides (e.g., SO_3 in the case of H_2SO_4).[34] Thus, the MSE model provides a suitable foundation for studying the behavior of acids in CO_2 environments.

To create a foundation for understanding and predicting the behavior of corrosive acids in CO_2 transportation systems, this study combines solubility measurements and thermodynamic modeling. For this purpose, experimental testing is carried out to determine the individual solubility of nitric and sulfuric acids in both liquid and supercritical CO_2 (i.e., in the dense phase). The examined temperatures are 25 and 48 °C with pressure ranging from 80 to 170 bar. Then, the solubilities are used to parametrize the MSE model for predicting the properties of acid−CO_2 mixtures.

2. MATERIALS AND METHODS

2.1. Experimental Section. The acid solubility was determined by first saturating the CO_2 phase with acid, followed by capturing the acid in water scrubbers, as schematically illustrated in Figure 1. The green arrows indicate the flow direction of CO_2. After a controlled amount of CO_2 had been fed through the system, the water from the scrubbers was analyzed for sulfate (in the case of sulfuric acid) and nitrate (in the case of nitric acid).

Table 1. Experimental Matrix[a]

	Nitric acid		Sulfuric acid	
	Temperature		Temperature	
Pressure (bar)	25 °C	50 °C	25 °C	50 °C
80		X		X
100	X	X	X	X
120		X		X
170		X		X

[a]The acids used were HNO_3 69% P.A. (1.01799.1000, MERCK) and H_2SO_4 95%−97% P.A. (1.00731.1000).

A mass flow controller was used to give a constant CO_2 flow. The CO_2 reservoir (autoclave) was placed on a scale to confirm the total amount of CO_2 as weight change. The CO_2 reservoir was a single piston cylinder with nitrogen back pressure, which also set the pressure for the whole system.

The CO_2 entered first an expansion tank (1), which worked as a pressure buffer and a safety reservoir to prevent the acid from getting pushed into the CO_2 source reservoir in case of accidental back-flow. Then the CO_2 was led into the first acid saturation cell (2), which consisted of a glass tube inside a SS316 autoclave, where glass wool was used as restriction in the glass tube to ensure the longest possible contact time between the dense phase CO_2 and the acid. After the second acid saturation cell (3), the CO_2 passed through the acid droplet fall-out tank (4) which also was filled with glass wool to prevent the entrained acid droplets from moving further and to ensure that only CO_2 with dissolved acid went to the main acid scrubber (5). The water level in the main acid scrubber was about 85% full, and a magnetic stirrer (6) was used to achieve good mixing of CO_2 and water. A second acid scrubber (8) captured the remains of the acid in the CO_2. The CO_2 was finally vented out after depressurisation with a heated pressure regulator. To ensure an even uptake of acid in the acid scrubber during the experiment, a conductivity probe (7) was used for monitoring. This was designed to eliminate experiments with unwanted acid carry over. Experiments with a sudden change in conductivity was discarded.

Using both a mass flow controller and weight control of the CO_2 source gave a good control of the total mass of CO_2 that had passed through the system. A deviation between these two numbers would indicate experimental artifacts such as leakage.

The acid solubility was calculated as the total amount of sulfate/nitrate (mol) found in both acid scrubbers divided by the total amount (kg) of CO_2 passing through the system

$$C_{solu} = \frac{C_{Acid,w} \times m_w}{m_{CO_2} \times MW_{Acid}} \quad (1)$$

where C_{solu} is the solubility in mmol/kg, $C_{Acid,w}$ is the measured concentration of anions in the water scrubbers as mg/kg, m_w is the mass of water in the scrubbers in kg, MW_{Acid} is the molecular weight of the acid, and m_{CO2} is the mass of CO_2 passing through the acid setup in kg.

The acid setup was placed inside a cabinet with temperature control. The pressure was controlled with nitrogen back pressure, which could be adjusted between 50 to 200 bar with a pressure controller that had an accuracy of ±0.1 bar. Before the experiments were started, the water in the acid scrubber was saturated with pure CO_2 (99.999%) to ensure constant flow of CO_2 when the experiment was started.

The mass flow controller was mounted after the heated gas regulator just before the venting stage and kept constant flow. The retention time through the acid uptake process was about 3 h, slightly depending on pressure and temperature. The acid scrubber retention time was between 8 to 12 h.

The water (osmotic) in the acid scrubbers was changed between every experiment, and the sulfate and nitrate contents in the water were analyzed with ion chromatography (IC). The scrubber was washed with osmotic water by filling its volume at least 10 times before each experiment.

It was not necessary to change the acid between all experiments; the nitric acid was changed every 10th time, while the sulfuric acid was used up to 50 times (since its solubility was so much lower). Normally, 200 to 1200 g of CO_2 were used for each experiment. A summary of the experimental parameters is shown in Table 1.

2.2. Modeling. The Mixed-Solvent Electrolyte (MSE) thermodynamic framework was derived by Wang et al.[31,34] and further extended by Springer et al.[32] to CO_2-containing systems in wide ranges of pressure and temperature. A brief summary of the model and the parameters that need to be

DOI: 10.1021/acs.iecr.9b04957
Ind. Eng. Chem. Res. 2019, 58, 22924−22933

evaluated in order to reproduce the behavior of acids in CO_2 is given in the following paragraphs.

To model CO_2 systems that may be in equilibrium with additional phases (such as concentrated acid phases), it is necessary to consider speciation reactions in the liquid phase. The fundamental reactions for CO_2 are given by

$$CO_2 + 2H_2O = H_3O^+ + HCO_3^- \quad (2)$$

$$HCO_3^- + H_2O = H_3O^+ + CO_3^{2-} \quad (3)$$

and are accompanied by the self-dissociation of water, i.e.,

$$2H_2O = H_3O^+ + OH^- \quad (4)$$

The acids also undergo acid−base reactions. In the case of sulfuric acid, the reactions are

$$H_2SO_4 + H_2O = HSO_4^- + H_3O^+ \quad (5)$$

$$HSO_4^- + H_2O = SO_4^{2-} + H_3O^+ \quad (6)$$

$$H_2SO_4 = H_2O + SO_3 \quad (7)$$

Similar acid−base reactions are considered for nitric acid:

$$HNO_3 + H_2O = NO_3^- + H_3O^+ \quad (8)$$

$$2HNO_3 = H_2O + N_2O_5 \quad (9)$$

In addition to chemical speciation equilibria, the model includes vapor−liquid equilibria for all neutral species that may partition between vapor and liquid phases, i.e.,

$$A_i^L = A_i^G \quad (10)$$

where A_i denotes any species that may exist in both the liquid and gas phases, and the superscripts L and G identify the liquid and gas phases, respectively. As the pressure increases, vapor−liquid equilibria may transition into liquid−liquid equilibria. Thus, liquid−liquid equilibria are also considered, i.e.,

$$A_i^{L1} = A_i^{L2} \quad (11)$$

where the superscripts L1 and L2 identify two coexisting liquid phases.

Phase equilibria and chemical speciation equilibria between aqueous species are calculated using the chemical potential as described earlier.[32] The chemical potential of a species i in a liquid phase is calculated as

$$\mu_i^L = \mu_i^{L,0,m}(T, P) + RT \ln \frac{1000}{M_{H_2O}} + RT \ln x_i \gamma_i^{x,*}(T, P, \boldsymbol{x}) \quad (12)$$

where $\mu_i^{L,0,m}(T, P)$ is the molality-based standard-state chemical potential, x_i is the mole fraction, $\gamma_i^{x,*}(T, P, x)$ is the mole fraction-based activity coefficient, and M_{H_2O} is the molecular weight of water. The standard-state chemical potential is calculated as a function of temperature and pressure as described in previous studies.[31,32] The activity coefficients in eq 12 are obtained from an excess Gibbs energy formulation, which comprises three contributions

$$G^{ex} = G_{LR}^{ex} + G_{II}^{ex} + G_{SR}^{ex} \quad (13)$$

where G_{LR}^{ex} defines long-range electrostatic interactions, G_{II}^{ex} represents ion−ion and ion−molecule interactions, and G_{SR}^{ex} is a short-range interaction term. The G_{LR}^{ex} term is obtained from Pitzer's formulation of the Debye−Hückel model[35] and does not require adjustable parameters. The G_{II}^{ex} contribution is expressed as a function of composition as

$$\frac{G_{II}^{ex}}{RT} = -\left(\sum_i n_i\right) \sum_i \sum_j x_i x_j B_{ij}(I_x) \quad (14)$$

where $B_{ij}(I_x) = B_{ji}(I_x)$, $B_{ii} = B_{jj} = 0$, and the ionic strength dependence of B_{ij} is given by

$$B_{ij}(I_x) = b_{ij} + c_{ij} \exp(-\sqrt{I_x + a_1}) \quad (15)$$

In eq 15, a_1 has a fixed value,[32] and b_{ij} and c_{ij} are binary interaction parameters, which are obtained by regressing experimental data. The parameters b_{ij} and c_{ij} depend, in general, on temperature and pressure. The functional form of this dependence varies for particular chemical systems. The short-range interaction contribution is calculated from the UNIQUAC equation[36]

$$\frac{G_{SR}^{ex}}{RT} = \left(\sum_i n_i\right)\left[\sum_i x_i \ln \frac{\varphi_i}{x_i} + \frac{Z}{2} \sum_i q_i x_i \ln \frac{\theta_i}{\varphi_i}\right] - \left(\sum_i n_i\right)\left[\sum_i q_i x_i \ln\left(\sum_j \theta_j \tau_{ij}\right)\right] \quad (16)$$

The fractions θ_i and φ_i and the energetic parameters τ_i are defined as

$$\theta_i = \frac{q_i x_i}{\sum_j q_j x_j} \quad (17)$$

$$\varphi_i = \frac{r_i x_i}{\sum_j r_j x_j} \quad (18)$$

$$\tau_{ji} = \exp\left(-\frac{a_{ji}}{RT}\right) \quad (19)$$

where q_i and r_i are the surface and size parameters, respectively, Z is a fixed coordination number, and a_{ij} ($a_{ij} \neq a_{ji}$) are binary interaction parameters for neutral molecules. As with the b_{ij} and c_{ij} parameters, the parameters a_{ij} may depend on temperature and pressure for particular chemical systems.

The activity coefficients are calculated from eq 13 by differentiation with respect to the number of moles using standard thermodynamics and are further used in eq 12.

The chemical potential of species i in the gas phase is given by the standard relation

$$\mu_i^G = \mu_i^{G,0}(T) + RT \ln \frac{P y_i \phi_i(T, P)}{P^0} \quad (20)$$

where $\mu_i^{G,0}(T)$ is the chemical potential of pure component i in the ideal gas state, y_i is the mole fraction in the gas phase, $\phi_i(T, P)$ is the fugacity coefficient, P is the total pressure, and $P^0 = 1$ atm. The $\mu_i^{G,0}(T)$ term is calculated from pure-component thermochemical properties,[32] and the fugacity coefficient is obtained from the Soave−Redlich−Kwong (SRK) equation of state,[37] in which the parameters a and b are calculated using the classical quadratic mixing rules, i.e.,

$$a = \sum_i \sum_j x_i x_j (a_i a_j)^{1/2} (1 - k_{ij}) \quad (21)$$

DOI: 10.1021/acs.iecr.9b04957
Ind. Eng. Chem. Res. 2019, 58, 22924−22933

$$b = \sum_i x_i b_i \tag{22}$$

where the pure-component parameters a_i and b_i are calculated using the critical properties,[37] and the binary parameter k_{ij} may be regressed based on experimental data.

The expressions for the chemical potentials of species in the liquid and gas phases (eqs 12 and 20) are coupled with material balance and electroneutrality constraints and used for the simultaneous calculation of phase and chemical equilibria.[38,39]

3. RESULTS

The results are reported as ppm/ppb mole and mmol/kg. For analyzing the correlation between solubility and density, the density of the CO_2 bulk phase was calculated from the NIST chemistry WebBook, SRD 69,[40] and it was assumed that the presence of acid (up to some 1000 ppm mole) did not affect the bulk density.

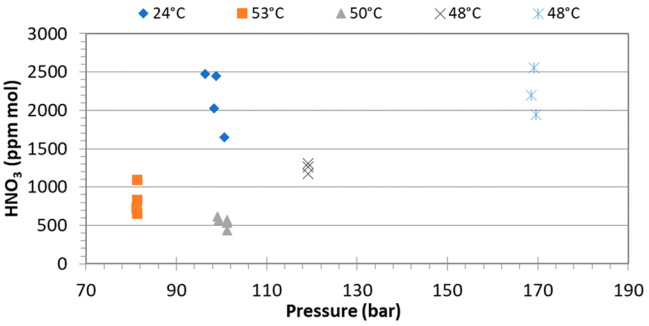

Figure 2. Solubility of nitric acid in dense phase CO_2 plotted as a function of pressure.

Table 3. Measured Solubility of Nitric Acid (Average Values) in Dense Phase CO_2

		Nitric acid solubility in dense phase CO_2			
Avg. temp. (°C)	Avg. pressure (bar)	Avg. (mmol/kg)	SD (mmol/kg)	Avg. (ppm mole)	SD (ppm mole)
24.1	98.6	49	8	2150	340
53.1	81.3	19	4	830	170
53.1	101.3	12	1	520	60
47.9	99.3	14	1	600	20
48.2	119.2	28	1	1250	60
48.1	169.1	51	6	2230	250

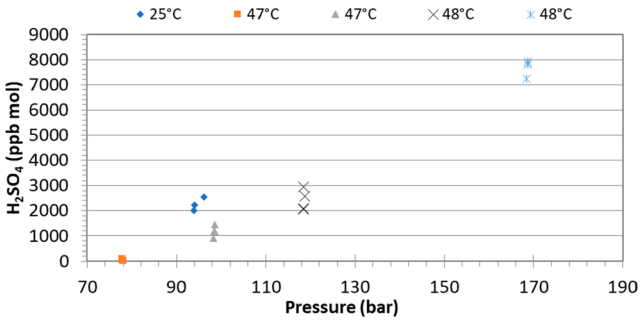

Figure 3. Measured solubility of sulfuric acid in dense phase CO_2 plotted as a function of pressure.

3.1. Measured Acid Solubilities. The results of nitric acid solubility measurements are summarized in Figure 2 and Table 2. The average temperature, pressure, and solubility values are shown in Table 3.

Table 2. Solubility of Nitric Acid in Dense Phase CO_2

			CO_2		measured NO_3^-		HNO_3 solubility	
Exp no.	Temp. (°C)	Pressure (bar)	mass (g)	density (kg/m^3)	(mg)	(mmole)	(ppm mole)	(mmol/kg)
1	23.4	96.4	845	825	2942.9	47.45	2471	56.15
2	25.1	98.8	715	815	2467.3	39.80	2449	55.66
3	23.8	98.4	590	825	1683.9	27.16	2025	46.03
4	24.2	100.7	885	825	2057.4	33.18	1650	37.5
5	52.5	81.3	210	217	247.1	3.97	835	18.98
6	53	81.3	310	216	476.8	7.69	1092	24.81
7	53.9	81.3	195	213	178.5	2.88	650	14.77
8	53	81.2	335	215	343.1	5.54	727	16.52
9	53	101.3	210	357	158.4	2.56	536	12.17
10	52.7	101.3	460	360	283.4	4.57	437	9.94
11	53.5	101.2	235	350	190.3	3.07	575	13.06
12	47.8	99.1	425	413	370.2	6.0	618	14.05
13	47.9	99.4	583	415	469.4	7.57	572	13.0
14	47.9	119.2	445	614	818.4	13.2	1305	29.66
15	48.2	119.2	480	608	793.9	12.8	1174	26.68
16	48.6	119.1	688	601	1222.8	19.72	1262	28.69
17	48.3	169.1	330	751	1189.1	19.18	2557	58.12
18	48.1	168.5	435	752	1346.6	21.72	2197	49.93
19	48	169.6	415	753	1139.9	18.39	1949	44.3

DOI: 10.1021/acs.iecr.9b04957
Ind. Eng. Chem. Res. 2019, 58, 22924−22933

Table 4. Solubility of Sulfuric Acid in Dense Phase CO_2

			CO_2		Measured SO_4^{2-}		H_2SO_4 solubility	
Exp no.	Temp. (°C)	Pressure (bar)	mass (g)	Density (kg/m^3)	mg	mmole	ppb mole	mmol/kg
20	25.4	93.8	1020	803	4.5946	0.0469	2022	0.04596
21	24.4	94	1000	813	4.9446	0.0505	2220	0.05045
22	25.3	96.1	790	808	4.4869	0.0458	2550	0.05796
23	47.1	77.8	410	218	0.095375	0.000973	108	0.00246
24	46.2	77.8	900	221	0.080665	0.000823	43	0.00098
25	46.3	78.1	900	223	0.045187	0.000461	25.8	0.00059
26	46.6	77.8	845	220	0.068985	0.000704	40	0.00091
27	46.4	77.8	1150	220	0.20951	0.002138	84	0.0019
28	46.7	98.2	835	425	1.503508	0.015342	907	0.02061
29	46.9	98.5	815	424	1.887671	0.019262	1163	0.02643
30	47.6	98.4	890	407	2.20252	0.022475	1179	0.02679
31	47.5	98.6	840	412	2.619496	0.02673	1456	0.03309
32	48.2	118.4	815	609	3.7428	0.03819	2062	0.04686
33	48.1	118.5	885	611	5.7958	0.05915	2941	0.06684
34	48.3	118.8	810	610	4.6578	0.04753	2582	0.05868
35	46.9	118.5	885	624	4.1032	0.04187	2082	0.04731
36	48.2	168.8	865	753	15.133	0.15441	7855	0.17851
37	48.6	168.4	405	750	6.5201	0.06653	7228	0.16428
38	48.3	168.8	720	753	12.714	0.12974	7928	0.18019
39	48.5	168.8	980	751	17.04	0.17387	7807	0.17742

Table 5. Measured Solubility of Sulfuric Acid (Average Numbers) in Dense Phase CO_2

		Sulfuric acid solubility in dense phase CO_2			
Avg. temp. (°C)	Avg. pressure (bar)	Avg. (mmol/kg)	SD (mmol/kg)	Avg. (ppb mole)	SD (ppb mole)
25.0	94.6	0.052	0.005	2260	220
46.5	77.9	0.0014	0.0007	60	30
47.2	98.4	0.027	0.004	1180	200
47.9	118.6	0.055	0.008	2400	370
48.4	168.7	0.175	0.006	7700	280

Table 6. Literature Data Sources for CO_2−H_2SO_4−H_2O Mixtures

Temp. (°C)	Pressure (atm.)	H_2SO_4 (mole fraction)	ref
17	1	0−1	Setschenow (1879)[41]
15, 25	1	0−0.17	Geffcken (1904)[42]
20	1	0−0.8	Christoff (1906)[43]
25	1	0−1	Markham and Kobe (1941)[44]
15−75	1	0−0.5	Shchennikova et al. (1957)[45]

Table 7. Literature Data Sources for CO_2−HNO_3−H_2O Mixtures

Temp. (°C)	Pressure (atm.)	HNO_3 (mole fraction)	ref
15, 25	1	0−0.05	Geffcken (1904)[42]
25	1	0−0.03	Onda et al. (1970)[46]

Table 8. Parameters of MSE Thermodynamic Model (cf. eqs 15, 19, and 21) for H_2SO_4−CO_2 Mixture

Species pair	Parameter	Value
CO_2/SO_4^{2-}	b_{ij}	45.6627
	c_{ij}	−50.3291
	a_{ij}	21,875−6.25333 P
CO_2/HSO_4^-	b_{ij}	6.35072
	c_{ij}	−14.6636
	a_{ij}	21,875−6.25333 P
$CO_2/H_2SO_4^0$	b_{ij}	−0.578787
	c_{ij}	0.312649
	a_{ij}	21,875−6.25333 P
	k_{ij}	0.16168

Table 9. Parameters of MSE Model (cf. eqs 15, 19, and 21) for HNO_3−CO_2 Mixture

Species pair	Parameter	Value
CO_2/NO_3^-	b_{ij}	2.05954
	a_{ij}	30,000 + (−73.4589 + 0.199313 T) P
CO_2/HNO_3^0	a_{ij}	10,155 + (−73.4589 + 0.199313 T) P
	k_{ij}	0.304953

The results of the sulfuric acid solubility measurements in dense phase CO_2 as a function of temperature and pressure are summarized in Figure 3 and Table 4. The average values of temperature, pressure, and solubility are shown in Table 5.

3.2. Modeling. To obtain a comprehensive thermodynamic model for acids in CO_2, it is necessary to reproduce not only the acid solubilities measured in this study, but also the solubilities of CO_2 in aqueous acid solutions. This is important to be able to model the phase assemblages in CO_2 transportation, in which droplets of acids exist within CO_2 environments. Furthermore,

DOI: 10.1021/acs.iecr.9b04957
Ind. Eng. Chem. Res. 2019, 58, 22924−22933

the simultaneous treatment of the acids in CO_2-rich phases as well as of CO_2 in acid (or water)-rich phases is necessary to obtain well-constrained and meaningful parameters of the thermodynamic model (cf. Section 2.1). Therefore, the available experimental data have been assembled from the literature for CO_2 solubility in aqueous acid solutions. These data are summarized in Tables 6 and 7 for H_2SO_4 and HNO_3 solutions, respectively.

The parameters of the MSE thermodynamic model have been obtained by jointly regressing the acid solubilities reported in this study and the CO_2 solubilities reported in the literature. For this purpose, the procedures described in previous studies[32,47] were used. The obtained interaction parameters between carbon dioxide and the relevant acid species are listed in Tables 8 and 9 for the H_2SO_4−CO_2 and HNO−CO_2 systems, respectively.

4. DISCUSSION

4.1. Experimental Results. The results showed that the acid solubility was, in general, much higher for nitric acid than for sulfuric acid, with a difference of about 3 orders of magnitude, as shown in Figure 4. There are no data available in the literature for acid solubility in dense phase CO_2 to compare with, but the vapor pressures of pure nitric acid and sulfuric acids have been measured in air. Gmitro and Vermeulen[48] reported the vapor pressure of sulfuric acid to be 10^{-3} mm Hg (~1.3 ppm mole) and 10^{-2} mm Hg (~13 ppm mole) at 25 and 50 °C, respectively. Sproesser and Taylor[49] reported vapor pressures for nitric acid of 6.2 (~8200 ppm mole) and 13.7 (~18,300 ppm mole) mm Hg at 35 and 50 °C, respectively. Thus, the vapor pressure of nitric acid in air is about 3 orders of magnitude higher than that of sulfuric acid. Although these vapor pressures were obtained at ambient total pressures in air, the ratios are in good agreement with our findings.

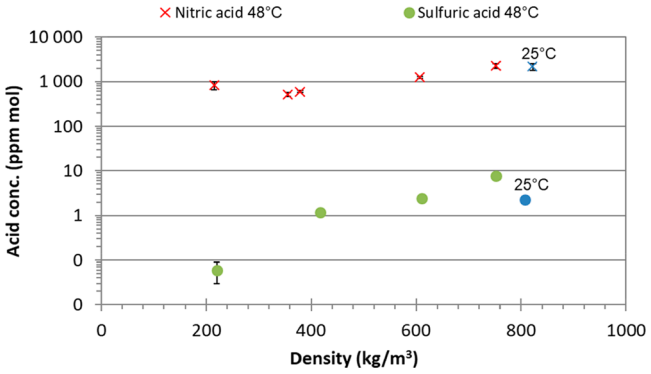

Figure 4. Comparison of sulfuric acid (round) and nitric acid (cross) solubility as a function of CO_2 density at 48 °C. The values are average numbers with standard deviation error bars. The markers in blue were measured at 25 °C.

For the same temperature, the sulfuric acid solubility was increasing with increasing pressure (Figure 3). At 78 bar, the solubility was very low (60 ± 30 ppb mole) but increased to 1000−2500 ppb mole when the pressure was increased to 95 bar or more. This large solubility increase caused by a relatively small pressure increase is believed to be related to the CO_2 phase changing from a vapor-like to a significantly denser, liquid-like supercritical state.

Nitric acid showed essentially the same trend as sulfuric acid with increasing solubility with increasing pressure (Figure 2) but with higher solubility around 80 bar and a shallow minimum around 100 bar. This can also be observed when the solubility is plotted as a function of CO_2 density (Figure 4), with a drop around 360 kg/m^3. The reason for this is not known, but it could possibly be related to property changes of the supercritical CO_2 when the pressure changes.

Figure 5 shows a comparison of different thermodynamic properties for CO_2 (at 25 and 48 °C). At 48 °C, the density increases gradually with increasing pressure, while the heat capacity (Cp) has a maximum at 100 bar and declines below and above this pressure. This shows that CO_2 can display some difference in properties at 100 bara and 48 °C, which fits well with the findings.

This might indicate that the transition between gas-like and liquid-like supercritical CO_2 above the critical point is not straightforward. Instead, there is a gradual change around 100 bara at 48 °C. This was not observed in the sulfuric acid experiment, but instead the lowest value was found around 80 bara. Since the solubility of sulfuric acid is much lower than the solubility of nitric acid, it could be expected that the presence of nitric acid would affect the CO_2 properties more than that of sulfuric acid.

The standard deviation (SD) is high for some of the data series, and this reflect the difficulties in measuring the solubility of acid at high CO_2 pressure. The lowest measured value of sulfuric acid, 60 ppb mole at 79 bara and 47 °C, had the highest

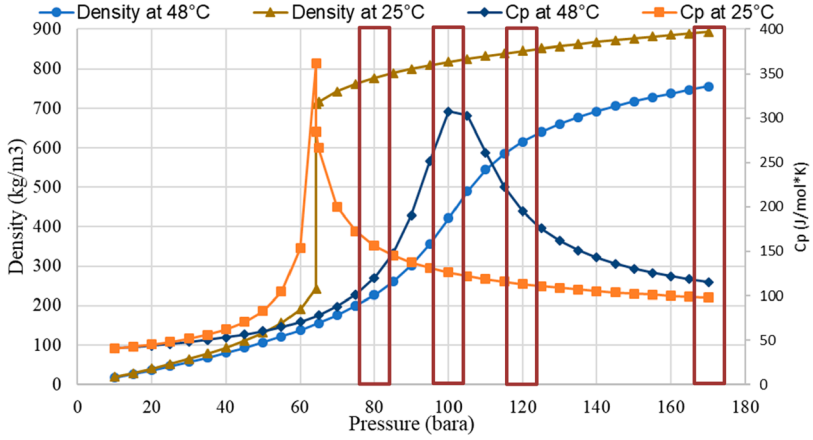

Figure 5. Thermophysical properties for CO_2 at 48 °C as a function of pressure, calculated using the NIST Chemistry WebBook, SRD 69.[40] The vertical rectangles indicate the pressures at which the solubility was measured.

DOI: 10.1021/acs.iecr.9b04957
Ind. Eng. Chem. Res. 2019, 58, 22924−22933

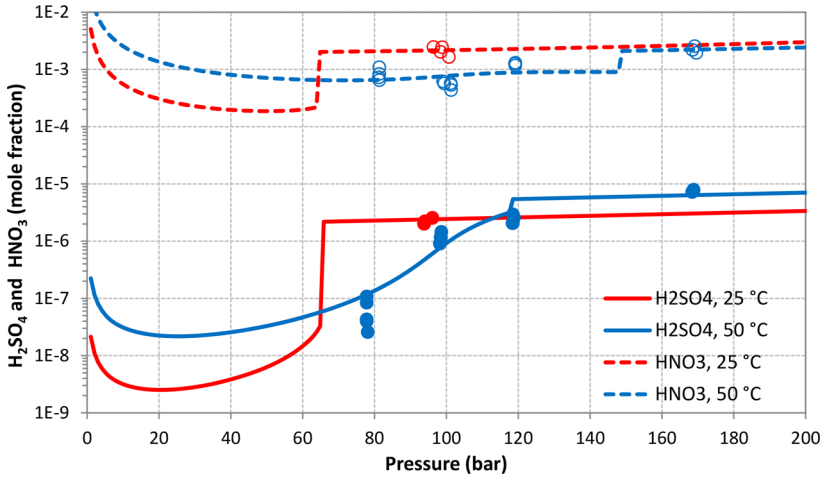

Figure 6. Comparison of calculated and experimental solubilities of sulfuric acid (solid lines, solid symbols) and nitric acid (dashed lines, hollow symbols) in CO_2. The lines show the MSE model calculations, whereas the symbols denote the experimental data.

SD. The complexity in the experimental setup makes it hard to predict an exact lower detection limit (LOD) for the system, but it is reasonable to assume that the lowest number are close to the LOD. This naturally affects their scattering. Even the scattered data are useful for validating the model, and in fact, the predicted lines go through some of the points in the region of high uncertainty (Figure 6).

4.2. Modeling vs Experimental Data. The results of calculations for the H_2SO_4−CO_2 and HNO_3−CO_2 systems are shown in Figure 6. The model represents the data with an accuracy that is close to the experimental scattering. It is evident that the pressure dependence of the solubility is quite complex. For both sulfuric acid (solid lines) and nitric acid (dashed lines) at 25 °C, an abrupt increase in solubility is observed at ∼65 bar. This is due to a transition between a gas-phase CO_2 environment below ∼65 bar and a liquid-phase environment above this pressure. However, the solubility values are very different for both acids. Below ∼65 bar, the mole fraction of H_2SO_4 is very low, i.e., of the order of 10^{-9} to 10^{-8}. At ∼65 bar, the solubility increases by about 2 orders of magnitude. This behavior is related to the low volatility of sulfuric acid. In the gas phase, the solvation of sulfuric acid is very weak, and therefore, the low volatility prevents the acid from being dissolved to a substantial degree. In the liquid-phase environment, the solvation of H_2SO_4 is appreciably higher and results in a higher solubility. It should be noted that an abrupt increase in solubility with pressure is well known for other solutes in subcritical CO_2. In particular, the solubility of water in subcritical CO_2 shows a similar increase, which has been verified in multiple experimental studies (cf. Springer et al.[32] and references cited therein). The solubility pattern is quite different at ∼50 °C, at which temperature CO_2 is a supercritical fluid. In this case, a much more gradual increase in solubility is observed for sulfuric acid because an increase in pressure is associated with a gradual transition from a vapor-like to a liquid-like solvent. The predictions show a small but noticeable transition at ∼118 bar, which is due to the fact that the model was constructed in the γ−φ framework and uses different mathematical formulations for the gas and liquid phases (cf. Section 2.1). In the liquid-like region at pressures above ∼118 bar, the pressure dependence of the solubility of H_2SO_4 is much weaker and is similar to the pressure dependence observed at 25 °C in the liquid region. An interesting feature of the 50 °C isotherm is the strong increase in solubility with pressure, i.e., by about 2 orders of magnitude from ∼78 to ∼170 bar. This is associated with a strong increase in the solvation of the acid as pressure increases, which solubilizes the relatively nonvolatile solute.

In the case of nitric acid (cf. dashed lines in Figure 6), the solubility pattern is qualitatively similar, but the solubility values are much higher. Nitric acid is much more volatile, and therefore, the mole fraction of nitric acid in the gas phase is ∼4 orders of magnitude higher than that of sulfuric acid. As with H_2SO_4, the HNO_3 concentration shows an abrupt increase at 25 °C and ∼65 bar, but this increase is not as strong as in the case of H_2SO_4 (i.e., by about 1 order of magnitude compared to 2 orders of magnitude for H_2SO_4). Since HNO_3 is much more volatile in the gas phase, the effect of increasing pressure (and at the same time increasing solvation) is not as strong as in the case of H_2SO_4. This is especially evident at 50 °C, where the pressure effect on solubility is much weaker for HNO_3. It is noteworthy that the predicted solubility isotherms show a crossover as a function of pressure. This seemingly counterintuitive behavior is not uncommon as it has been experimentally verified for the solubility of water in CO_2.[32] This pattern is due to the transition from the solubility in the gas phase to that in the liquid phase (or liquid-like supercritical phase).

4.3. Practical Significance. Crossing solubility lines could have important practical consequences for long CO_2 transport pipelines. It has been experimentally demonstrated that sulfuric and nitric acids may form in certain CO_2 blends as a result of chemical reactions between certain impurities. If these acids precipitate, they will form a separate liquid phase. The acids are known to be hygroscopic and could therefore absorb water from the CO_2 bulk phase and create a highly acidic, concentrated aqueous phase that is corrosive to carbon steel. Such a phase could pose a major integrity risk for the transportation system. However, if the acids that form remain dissolved in the CO_2, they can probably follow the CO_2 stream without affecting the transportation system. Limited amounts of acids, for example, formed during short upset conditions, could probably be removed later by dissolution ("drying out") in the CO_2 stream. If the acid solubility is reduced along the flow direction, for example, due to temperature or pressure changes, acids could precipitate at certain locations and cause corrosion, followed by the formation of solid corrosion products. Such a scenario is likely because it is usually expected that both the temperature

DOI: 10.1021/acs.iecr.9b04957
Ind. Eng. Chem. Res. 2019, 58, 22924−22933

and pressure will be reduced in the flow direction. Even if the amount of the acid phase is minute compared to the amount of the CO_2 phase, the acid phase is expected to readily drop out and accumulate on the metal surface due to the large difference between the densities of the acids and the CO_2 phase.

As shown in Figure 6, the solubility generally increases as the temperature is reduced at sufficiently high pressures (for both acids), so the temperature effect is probably not of too great concern. There is, however, some reduction of the sulfuric acid solubility when going from 50 to 25 °C at pressures in excess of 120 bar (Figure 6). For both acids, there is an abrupt solubility decrease when the pressure crosses a certain threshold that is associated with a change of phase state. Even if there is some spread in the results of the present work, it has been clearly demonstrated that for an acid-saturated CO_2 stream, precipitation could occur within the operational pressures that are expected for transport pipelines. This effect is probably of most significance for sulfuric acid because its solubility is so low, and the change with pressure is very high. The results of the present work could be used to predict if or where precipitation of acids could occur.

5. CONCLUSIONS

- To understand the potentially corrosive behavior of strong acids that may form in CO_2 transportation systems, the solubility of nitric acid and sulfuric acid in CO_2 was measured experimentally for different pressures (80−170 bar) and temperatures (25 and 48 °C).
- The solubilities varied with temperature and pressure, but in general, nitric acid is about 3 orders of magnitude more soluble than sulfuric acid.
- The experimentally measured solubilities have been used to parametrize a thermodynamic model that could be used to predict acid solubilities at conditions that go beyond the experimental conditions. Furthermore, it is expected that the model will be applicable to complex mixtures containing multiple impurities dissolved in CO_2.
- The experimental and modeling results indicated that both sulfuric acid and nitric acid dropout could occur within expected operational conditions for CO_2 transport pipelines.

AUTHOR INFORMATION

Corresponding Author

*E-mail: bjornhm@ife.no.

ORCID

Bjørn H. Morland: 0000-0002-6788-8425

Andre Anderko: 0000-0002-1522-4889

Notes

The authors declare no competing financial interest.

ACKNOWLEDGMENTS

The present work was carried out as part of the Kjeller Dense Phase CO_2 Corrosion II project (KDC-II). The authors would like to thank CLIMIT (Norwegian Research Council, project no. 243624/E20), Shell, Total, ArcelorMittal, OLI, and Gassco for financial and technical support.

REFERENCES

(1) *Energy Technology Perspectives 2010, Scenarios & Strategies to 2050*; IEA: Paris, 2010.

(2) Stocker, T. F., Qin, D., Plattner, G.-K., Tignor, M., Allen, S. K., Boschung, J., Nauels, A., Xia, Y., Bex, V., Midgley, P. M., Eds. Summary for Policymakers. In *Climate Change 2013: The Physical Science Basis. Contribution of Working Group I to the Fifth Assessment Report of the Intergovermmental Panel on Climate Change*; Cambridge University Press, Cambridge and New York, 2013.

(3) Yevtushenko, O.; Bettge, D.; Bäßler, R.; Bohraus, S. Corrosion of CO_2 transport and injection pipeline steels due to the condensation effects caused by SO_2 and NO_2 impurities. *Mater. Corros.* **2015**, *66* (4), 334−341.

(4) Morland, B. H.; Tjelta, M.; Dugstad, A.; Svenningsen, G. *Formation of Strong Acids in Dense Phase CO_2*. In *CORROSION/2018*; NACE International: Phoenix, AZ, 2018.

(5) Dugstad, A.; Morland, B. H., Formation of Corrosive Phases in Dense Phase CO_2. In *Eurocorr 2016*; Montpellier, France, 2016.

(6) Dugstad, A.; Halseid, M.; Morland, B. Testing of CO_2 specifications with respect to corrosion and bulk phase reactions. *Energy Procedia* **2014**, *63*, 2547−2556.

(7) Dugstad, A.; Halseid, M.; Morland, B. Effect of SO_2 and NO_2 on corrosion and solid formation in dense phase CO_2 pipelines. *Energy Procedia* **2013**, *37*, 2877−2887.

(8) Quynh Hoa, L.; Baessler, R.; Bettge, D. On the Corrosion Mechanism of CO_2 Transport Pipeline Steel Caused by Condensate: Synergistic Effects of NO_2 and SO_2. *Materials* **2019**, *12* (3), 364.

(9) Morland, B. H.; Norby, T.; Tjelta, M.; Svenningsen, G. Effect of SO_2, O_2, NO_2, and H_2O Concentrations on Chemical Reactions and Corrosion of Carbon Steel in Dense Phase CO_2. *Corrosion* **2019**, *75* (11), 1327−1338.

(10) Span, R.; Gernert, J.; Jager, A. Accurate Thermodynamic-Property Models for CO_2-Rich Mixtures. In *Ghgt-11*; Dixon, T., Yamaji, K., Eds.; Elsevier Science Bv: Amsterdam, 2013; Vol. *37*, pp 2914−2922.

(11) Munkejord, S. T.; Hammer, M.; Lovseth, S. W. CO_2 transport: Data and models - A review. *Appl. Energy* **2016**, *169*, 499−523.

(12) Trusler, J. P. M. Thermophysical Properties and Phase Behavior of Fluids for Application in Carbon Capture and Storage Processes. *Annu. Rev. Chem. Biomol. Eng.* **2017**, *8*, 381−402.

(13) Bui, M.; Adjiman, C. S.; Bardow, A.; Anthony, E. J.; Boston, A.; Brown, S.; Fennell, P. S.; Fuss, S.; Galindo, A.; Hackett, L. A.; Hallett, J. P.; Herzog, H. J.; Jackson, G.; Kemper, J.; Krevor, S.; Maitland, G. C.; Matuszewski, M.; Metcalfe, I. S.; Petit, C.; Puxty, G.; Reimer, J.; Reiner, D. M.; Rubin, E. S.; Scott, S. A.; Shah, N.; Smit, B.; Trusler, J. P. M.; Webley, P.; Wilcox, J.; Mac Dowell, N. Carbon capture and storage (CCS): the way forward. *Energy Environ. Sci.* **2018**, *11* (5), 1062−1176.

(14) Kunz, O.; Wagner, W. The GERG-2008 Wide-Range Equation of State for Natural Gases and Other Mixtures: An Expansion of GERG-2004. *J. Chem. Eng. Data* **2012**, *57* (11), 3032−3091.

(15) Gernert, J.; Span, R. EOS-CG: A Helmholtz energy mixture model for humid gases and CCS mixtures. *J. Chem. Thermodyn.* **2016**, *93*, 274−293.

(16) Barta, L.; Bradley, D. J. Extension of the specific interaction model to include gas solubilities in high-temperature brines. *Geochim. Cosmochim. Acta* **1985**, *49* (1), 195−203.

(17) Rumpf, B.; Nicolaisen, H.; Ocal, C.; Maurer, G. Solubility of carbon dioxide in aqueous solutions of sodium chloride: Experimental results and correlation. *J. Solution Chem.* **1994**, *23* (3), 431−448.

(18) Duan, Z. H.; Sun, R. An improved model calculating CO_2 solubility in pure water and aqueous NaCl solutions from 273 to 533 K and from 0 to 2000 bar. *Chem. Geol.* **2003**, *193* (3−4), 257−271.

(19) Duan, Z. H.; Sun, R.; Zhu, C.; Chou, I. M. An improved model for the calculation of CO_2 solubility in aqueous solutions containing Na^+, K^+, Ca^{2+}, Mg^{2+}, Cl^-, and SO_4^{2-}. *Mar. Chem.* **2006**, *98* (2−4), 131−139.

(20) Akinfiev, N. N.; Diamond, L. W. Thermodynamic model of aqueous CO_2-H_2O-NaCl solutions from-22 to 100 C and from 0.1 to 100 MPa. *Fluid Phase Equilib.* **2010**, *295* (1), 104−124.

(21) Li, Y. K.; Nghiem, L. X. Phase equilibria of oil, gas and water brine mixtures from a cubic equation of state and Henry law. *Can. J. Chem. Eng.* **1986**, *64* (3), 486−496.

DOI: 10.1021/acs.iecr.9b04957
Ind. Eng. Chem. Res. 2019, 58, 22924−22933

(22) Li, J.; Duan, Z. A thermodynamic model for the prediction of phase equilibria and speciation in the H_2O-CO_2-NaCl-$CaCO_3$-$CaSO_4$ system from 0 to 250 degrees C, 1 to 1000 bar with NaCl concentrations up to halite saturation. *Geochim. Cosmochim. Acta* **2011**, *75* (15), 4351−4376.
(23) Spycher, N.; Pruess, K. CO_2-H_2O mixtures in the geological sequestration of CO_2. II. Partitioning in chloride brines at 12−100 C and up to 600 bar. *Geochim. Cosmochim. Acta* **2005**, *69* (13), 3309−3320.
(24) Li, J.; Wei, L. L.; Li, X. C. *Modeling of CO_2-CH_4-H_2S-brine based on cubic EOS and fugacity-activity approach and their comparisons*. In 12th International Conference on Greenhouse Gas Control Technologies, Ghgt-12, Dixon, T., Herzog, H., Twinning, S., Eds.; Elsevier Science Bv: Amsterdam, 2014; Vol. *63*, pp 3598−3607.
(25) Li, J.; Wei, L. L.; Li, X. C. An improved cubic model for the mutual solubilities of CO_2-CH_4-H_2S-brine systems to high temperature, pressure and salinity. *Appl. Geochem.* **2015**, *54*, 1−12.
(26) Harvey, A. H.; Prausnitz, J. M. Thermodynamics of high-pressure aqueous systems containing gases and salts. *AIChE J.* **1989**, *35* (4), 635−644.
(27) Ji, X. Y.; Tan, S. P.; Adidharma, H.; Radosz, M. SAFT1-RPM approximation extended to phase equilibria and densities of CO_2-H_2O and CO_2-H_2O-NaCl systems. *Ind. Eng. Chem. Res.* **2005**, *44* (22), 8419−8427.
(28) Tan, S. P.; Adidharma, H.; Radosz, M. Statistical associating fluid theory coupled with restricted primitive model to represent aqueous strong electrolytes. *Ind. Eng. Chem. Res.* **2005**, *44* (12), 4442−4452.
(29) Li, J. D.; Topphoff, M.; Fischer, K.; Gmehling, J. Prediction of gas solubilities in aqueous electrolyte systems using the predictive Soave-Redlich-Kwong model. *Ind. Eng. Chem. Res.* **2001**, *40* (16), 3703−3710.
(30) Kiepe, J.; Horstmann, S.; Fischer, K.; Gmehling, J. Experimental determination and prediction of gas solubility data for CO_2 + H_2O mixtures containing NaCl or KCl at temperatures between 313 and 393 K and pressures up to 10 MPa. *Ind. Eng. Chem. Res.* **2002**, *41* (17), 4393−4398.
(31) Wang, P. M.; Anderko, A.; Young, R. D. A speciation-based model for mixed-solvent electrolyte systems. *Fluid Phase Equilib.* **2002**, *203* (1−2), 141−176.
(32) Springer, R. D.; Wang, Z.; Anderko, A.; Wang, P.; Felmy, A. R. A thermodynamic model for predicting mineral reactivity in supercritical carbon dioxide: I. Phase behavior of carbon dioxide − water − chloride salt systems across the H_2O-rich to the CO_2-rich regions. *Chem. Geol.* **2012**, *322*−*323*, 151−171.
(33) Springer, R. D.; Wang, P.; Anderko, A. Modeling the properties of H_2S - CO_2 - salt - water systems in wide ranges of temperature and pressure. *SPE Journal* **2015**, *20* (5), 1120−1134.
(34) Wang, P.; Anderko, A.; Springer, R. D.; Young, R. D. Modeling phase equilibria and speciation in mixed-solvent electrolyte systems: II. Liquid-liquid equilibria and properties of associating electrolyte solutions. *J. Mol. Liq.* **2006**, *125* (1), 37−44.
(35) Pitzer, K. S. Electrolytes - from dilute solutions to fused salts. *J. Am. Chem. Soc.* **1980**, *102* (9), 2902−2906.
(36) Abrams, D. S.; Prausnitz, J. M. Statistical thermodynamics of liquid mixtures - new expressions for excess Gibbs energy of partly or completely miscible systems. *AIChE J.* **1975**, *21* (1), 116−128.
(37) Soave, G. Equilibrium Constants from a Modified Redlich-Kwong Equation of State. *Chem. Eng. Sci.* **1972**, *27* (6), 1197−1203.
(38) Zemaitis, J. F., Jr.; Clark, D. M.; Rafal, M.; Scrivner, N. C. *Handbook of Aqueous Electrolyte Thermodynamics*; American Institute of Chemical Engineers: New York, 1986.
(39) Anderko, A.; Wang, P.; Rafal, M. Electrolyte solutions: From thermodynamic and transport property models to the simulation of industrial processes. *Fluid Phase Equilib.* **2002**, *194*, 123−142.
(40) Linstrom, P. J., Mallard, W. G., Eds.; *NIST Chemistry WebBook, NIST Standard Reference Database Number 69*; National Institute of Standards and Technology: Gaithersburg, MD, 2011.
(41) Setchenow, J. *Mem. Academy Imp. Science*, 7th Ser; St. Petersbourg, 1879, *26* (13), 1−62.
(42) Geffcken, G. Articles on Knowledge of Solubility Influencing. *Z. Phys. Chem., Stoechiom. Verwandtschaftsl.* **1904**, *49* (3), 257−302.
(43) Christoff, A. On the Dependence of the Absorption on the Surface Tension. *Z. Phys. Chem., Stoechiom. Verwandtschaftsl.* **1906**, *55* (5), 622−634.
(44) Markham, A. E.; Kobe, K. A. The solubility of carbon dioxide and nitrous oxide in aqueous salt solutions. *J. Am. Chem. Soc.* **1941**, *63* (2), 449−454.
(45) Shchennikova, M. K.; Devyatykh, G. G.; Korshunov, I. A. *Russian Journal of Applied Chemistry* **1957**, *30* (6), 881−886.
(46) Onda, K.; Sada, E.; Kobayashi, T.; Kito, S.; Ito, K. Salting - out parameters of gas solubility in aqueous salt solutions. *J. Chem. Eng. Jpn.* **1970**, *3* (1), 18−24.
(47) Wang, P.; Anderko, A.; Young, R. D. A speciation-based model for mixed-solvent electrolyte systems. *Fluid Phase Equilib.* **2002**, *203* (1−2), 141−176.
(48) Gmitro, J. I.; Vermeulen, T. Vapor-liquid equilibria for aqueous sulfuric acid. *AIChE J.* **1964**, *10* (5), 740−746.
(49) Sproesser, W. C.; Taylor, G. B. J. Vapor pressures of aqueous solutions of nitric acid. *J. Am. Chem. Soc.* **1921**, *43* (8), 1782−1787.

DOI: 10.1021/acs.iecr.9b04957
Ind. Eng. Chem. Res. 2019, 58, 22924−22933